INTERNATIONAL JOURNAL OF GEOMAGNETISM AND AERONOMY
VOL. 6, GI3001, doi:10.1029/2005GI000114, 2006

Scattering of VLF field at a three-dimensional ionospheric irregularity: Investigation and application to the "Trimpi" problem

E. V. Moskaleva, and O. V. Soloviev

Institute of Radio Physics, St. Petersburg State University, St. Petersburg, Russia

Received 26 April 2005; revised 14 November 2005; accepted 25 April 2006; published 16 August 2006.

[1] This paper is devoted to mathematical simulation of the "Trimpi" effect on the base of the investigations of VLF field diffraction at a three-dimensional irregularity in the lower ionosphere. The problem of the field of a vertical electric dipole in a plain waveguide with homogeneous properties of the Earth's surface and inhomogeneous ionospheric wall is considered. The irregular impedance model of the waveguide is created using the known vertical profiles of the electron concentration and effective collision frequency. The modeled ionospheric irregularity is considered as a finite cylinder without any limitations to its shape and the dimensions of its base. An original asymptotic method using the apparatus of integral equations is used for solving the diffraction problem. On the basis of the numerical simulations performed, one can draw the following conclusions: not only the forward scatter of the field but the backscatter as well are observed; the irregularity impact depends on the propagation path orientation relative to the geomagnetic field, on the underlying surface properties, and the irregularity location and its geometric dimensions. The found field variations are of a significant character and can be detected experimentally. *INDEX TERMS:* 6964 Radio Science: Radio wave propagation; 2439 Ionosphere: Ionospheric irregularities; 2494 Ionosphere: Instruments and techniques; *KEYWORDS:* Wave propagation; Lower ionosphere; Ionospheric irregularity.

Citation: Moskaleva, E. V., and O. V. Soloviev (2006), Scattering of VLF field at a three-dimensional ionospheric irregularity: Investigation and application to the "Trimpi" problem, *Int. J. Geomagn. Aeron., 6,* GI3001, doi:10.1029/2005GI000114.

1. Introduction

[2] The scientific community pays (especially in the recent years) a great attention to studies of the phenomena related to thunderstorm activity. It became clear relatively recently that many of these phenomena are accompanied by local changes in the properties of the lower ionosphere (electron concentration and collision frequency). These changes should influence the propagation of VLF signals [*Dowden et al.*, 1994; *Inan et al.*, 1991, 1995]. Because of that, the "Trimpi" effect may be interpreted as a result of the scatter of the electromagnetic field propagating in the wavequide Earth–ionosphere at a local irregularity in the lower ionosphere. The goal of this paper is a mathematical simulation of the Trimpi effect which is a short-time variation in the amplitude and phase of VLF signal caused by appearance of a local three-dimensional perturbation in the lower ionosphere. The experimental recordings of the amplitude and phase of VLF signals published by *Nunn* [1996] show that sudden changes in the amplitude and phase may reach 6 dB and 10°, respectively. Such phenomena as heating of the ionosphere by electromagnetic pulse of the lightning [*Inan et al.*, 1991], energetic electron precipitation [*Rycroft,* 1973], and "cloud–ionosphere discharges" [*Dowden et al.*, 1994] may be causes of such changes. The Trimpi effect related to sprites (what can be also considered as three-dimensional irregularities of the propagation medium) attracts increased interest especially recently [*Rodger*, 2003]. Sprites are rather rare phenomena and it is still impossible to reproduce them in laboratory, so for their studies all possible methods should be studied including the VLF remote sounding method observing and studying variations in the fields of permanently operating VLF transmitters.

[3] Numerical simulation of the process of low-frequency electromagnetic wave propagation in the Earth–ionosphere waveguide in the presence of a local three-dimensional irregularity (the scattering properties of which should correspond to the currently available information on the plasma formations in the lower ionosphere) may help in choosing between this or that theory proposed to describe the causes and de-

1524–4423/06/2005GI000114$18.00

velopment of the above noted phenomena. The available observations do not provide complete information on the nature of such phenomena, and their principal parameters are known fairly approximately. One may state definitely that such irregularity is located in the region ∼50–90 km over the Earth's surface, that is, in the vicinity of the lower boundary of the ionosphere where its least ionized layers are located. So, if one identifies the appearance of the Trimpi effect with a sudden appearance of a three-dimensional local irregularity in the lower ionosphere, the variations in the amplitude and phase of the received signal at a particular radio wave propagation path may be explained by the scatter of radio waves at such irregularity. In this case one has to assume that the irregularity is characterized by increased (relative to the surrounding medium) charged particle concentration and probably by higher temperature (which fact may be interpreted as an increase in the effective collision frequency of electrons).

[4] Two types of the Trimpi effect are described in publications. The first one is a classical Trimpi effect [*Helliwell et al.*, 1973]. It is assumed to be a result of whistlers caused by energetic electron precipitations [*Rycroft,* 1973]. Part of the electromagnetic pulse energy the source of which was a lightning discharge may propagate with small losses along the geomagnetic field lines reflecting from the ionospheric boundary in the magnetically conjugated points and interacting to energetic electrons at the geomagnetic equator. The latter process may lead to the transfer of part of the energy from electrons to the electromagnetic wave. The electrons that have lost part of their energy are precipitating into the lower ionosphere altering its properties [*Rycroft*, 1973]. The classical Trimpi effect is characterized by some delay after the formation of a spherical (∼0.6 s) and rather long relaxation time (up to 100 s) [*Rodger*, 2003].

[5] The so-called "Early Trimpi" has much shorter delay (less than 100 μs) between the lightning discharge and registration of the disturbance [*Inan et al.*, 1988]. *Dowden et al.* [1996] and *Rodger* [2003] supposed that the ionospheric disturbances related to sprites and elves are manifested in the form of Early Trimpi. The Trimpi effect caused by sprites has a typical logarithmic decrease in time [*Dowden and Rodger*, 1997].

[6] Cloud–ionosphere discharges [*Winckler*, 1995] was one of the initially used terms for red sprites discovered in 1989 [*Franz et al.*, 1990]. Sprites are manifested in the form of light flashes observed over the thunderstorm clouds. It is interesting that for a human eye these flashes look red only in 37.5% of the cases (in other cases they look rose, orange, or even green) [*Lyons*, 1996]. These picturesque phenomena [*Dowden et al.,* 1997; *Lyons*, 1994; *Rairden and Mende*, 1995; *Sentman and Wescott,* 1995; *Winckler et al.*, 1996] immediately attracted common attention. However, their study appeared to be a rather complicated problem due to their low optical brightness [*Stenbaek-Nilsen et al.*, 2000] and short lifetime equal to tens of milliseconds [*Lyons*, 1996]. Probably that is why their observations are registered only at night. Theoretically, it is possible to observe sprites by a naked eye but only in exceptional cases. So to study these phenomena special optical systems are used [*Rairden and Mende,* 1995; *Sentman and Wescott*, 1995]. By their appearance sprites may be subdivided to the following types: "similar to a carrot", "having the shape of a column or "jelefish" [*Rodger*, 1999]. Their occurrence is usually related to strong (>50 kA) lightning discharges between a cloud and the surface of positive polarity (+CG) [*Boccippio et al.*, 1995; *Winckler*, 1995]. Sprites are generated at a height of about 50 km, that is, approximately by 30 km above the thunderstorm cloud. Their upper boundary is located at a height of about 90 km over the Earth's surface. The horizontal diameter of sprites (in the case when there are not less than two "columns") is 25–50 km [*Rodger*, 1999]. The frequency of sprite generation is rather low. Over the entire globe, lightning discharges occur 50–100 times per minute, but only a few are accompanied by sprites. The causes of this are, first, the fact that the lightning discharges of the positive polarity occur much more seldom than the discharges of negative polarity (10% "+CG" and 90% "−CG") [*Uman*, 1987]. Second, all sprites are related to strong positive discharges, whereas only in rare cases strong positive discharges are accompanied by these phenomena. Appearance of sprites has been detected in various climatic conditions both over the land and seas [*Boeck et al.*, 1995; *Vaughan et al.*, 1992].

[7] There exist various theories of the sprite generation mechanism. It is assumed that the electromagnetic pulse accompanying a lightning discharge (EMP), or the quasi-electrostatic field (QE) may be the cause of their generation [*Pasko et al.*, 1997; *Rowland et al.*, 1995; *Valdivia et al.,* 1997].

[8] Besides red sprites, such events as blue jets and elves are observed over thunderstorm clouds. Blue jets appear directly over the center of a thunderstorm cloud and are a narrow upward cone. Being born at the height of the upper boundary of the cloud (about 20 km), they reach a height of about 40–50 km over the Earth's surface spreading away in their upper part to the dimension of about 5 km with the cone aperture angle of about 15°. There exists a theory assuming that the blue jets initial stage is blue starters. They also present cones covering the region from approximately 17 km (the upper boundary of the cloud) to 25 km over the Earth's surface and in their upper part have a width of about 2 km. It was detected that they are generated in the vicinity of negative charges [*Wescott et al.*, 1996].

[9] The phenomena called elves are observed at altitudes of about 75–105 km after strong lightning discharges. [*Fukunishi et al.*, 1996a, 1996b]. It is assumed that these formations having the diameter of 100–300 km occur due to the heating of the electrons in the lower ionosphere by the electromagnetic pulse of the lightning discharge [*Inan et al.*, 1996].

[10] Many authors paid attention to studies of the Trimpi effect. A fairly detailed review of these studies was presented by *Soloviev and Hayakawa* [2002], who analyzed various methods of solution of the three-dimensional problems in the radio wave propagation theory. As far as we know from the publications, currently nothing cardinally new can be added to the list presented earlier. This paper presents a development of the studies begun by *Soloviev and Hayakawa* [2002]. Unlike in the latter paper, in this paper the influence of the geomagnetic field in the problem of diffraction at a three-dimensional irregularity is considered. This influence in the considered frequency range is most strongly

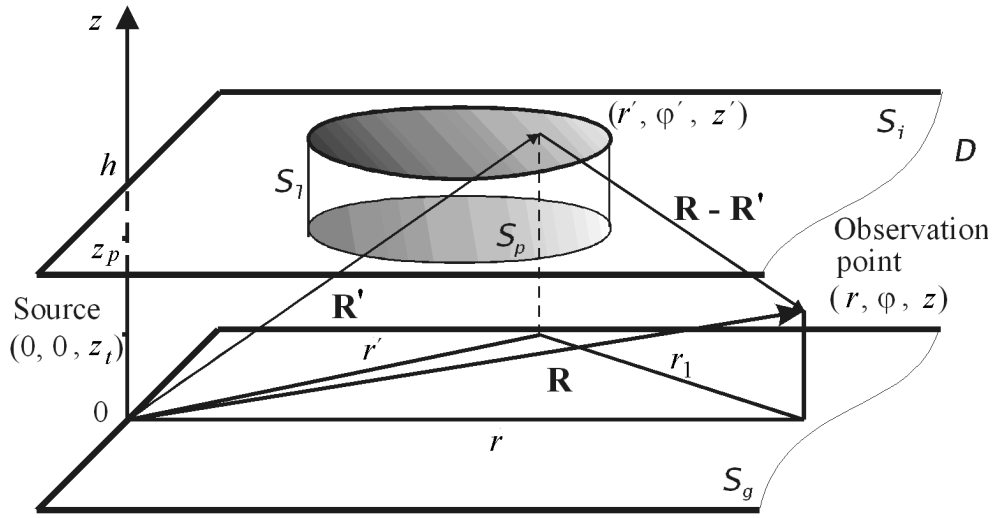

Figure 1. Geometry of the problem.

manifested at night when all sprites described in publications were optically observed.

[11] In this paper to solve the problem on the field of a vertical electric dipole in the Earth–ionosphere waveguide having a local irregularity at the upper wall, an original method based on the integral equations theory [*Soloviev and Hayakawa*, 1997] is applied. The irregularity is chosen in the form of a finite by height cylinder without any limitations on the shape and dimensions of its cross section. Though in publications there are indications to a presence of a fine structure of the sprites, this model does not take into account such structure, but models a sprite as a scattering volume. It is evident that using VLF electromagnetic field with a wavelength of the order of 15 km (for a frequency of 20 kHz) one cannot resolve the fine structure of a sprite. The scatter from the system of close-located "columns" would not differ from the scatter at the whole cylinder.

2. Formulation of Electrodynamical Problem of Scattering

[12] The problem of the field of a harmonic ($\exp(-i\omega t)$) vertical electric dipole in the Earth–ionosphere waveguide with a three-dimensional local irregularity is considered in the impedance formulation for the parallel-plain model of the waveguide channel. The published estimates of the vertical and horizontal dimensions of sprites modeled by our local irregularity show that the dimensions do not exceed 50–100 km. This means that the electromagnetic field scattered at such irregularity may be considerable (and thus may be observed and registered) only at short paths of ∼1000–1500 km for which one can neglect the curvature of the Earth's surface. The neglecting by the Earth's curvature makes the problem visual not breaking the general character of the proposed solution algorithm. A transition to the spherical model may be done using the formulae obtained by *Soloviev* [1990] and *Soloviev and Agapov* [1997]. In the considered model of the waveguide, the lower wall described by a plain surface S_g is assumed to be homogeneous, its properties being determined by the surface impedance δ_g. The waveguide is limited from the top by the surface S_i, its properties being determined (in its regular part) by the impedance δ_i. The three-dimensional local irregularity directly adjoining the upper wall of the waveguide is chosen in the form of a finite by a height cylinder, the shape of the cross section of it being arbitrary. The surface of the upper wall of the cylinder coincides with the surface S_i, whereas the surface of the lower wall S_p is located in the plane parallel to the surface S_i. We will denote the side surface of the cylinder as S_l. The properties of the waveguide space $D \in R^3$ limited by the waveguide walls and surfaces of the model irregularity coincide with the properties of the vacuum, its dielectric and magnetic permeability and wave number being ε_0, μ_0, and k, respectively.

[13] In the cylindrical coordinate system (r, φ, z) with the z axis going through the source, the surfaces S_g and S_i are described by the equations $z = 0$ and $z = h$, respectively. The source of the field (a vertical electrical dipole with the dipole moment P_0) is located in the point $(0, 0, z_t)$. The surface S_p lies in the plane $z = z_p$, and the surface S_l is parallel to the z axis. The problem geometry is shown in Figure 1. In a scalar approximation (neglecting field depolarization at the scatter at the three-dimensional irregularity) the electromagnetic field excited by such source is described by the vertical component of the Hertz vector which in the D region satisfies the inhomogeneous Helmholtz equation and the following boundary conditions:

$$\frac{1}{\Pi}\frac{\partial \Pi}{\partial n} = ik\delta(M)\Big|_{M \in S_g, S_i, S_l, S_p} \quad (1)$$

where n is the external normal to the boundary surfaces of the waveguide volume, $\delta(M) = \delta_g$ for $M \in S_g$, $\delta(M) = \delta_i$ for $M \in S_i$, $\delta(M) = \delta_l$ for $M \in S_l$, and $\delta(M) = \delta_p(r, \varphi)$ for $M \in S_p$. Conditions at the infinity require attenuation of $\Pi(r, \varphi, z)$ at $r \to \infty$. In this case there is no need to attract additionally a boundary condition at the edge (the line of crossing of S_p and S_i, S_p, and S_l) because the available conditions guarantee unambiguousness of the solution. It should be noted that actually in the VLF range, there are the following estimates of the impedance values for the TM polarization field generated by the considered source: $|\delta_{g,i,p}| < 1$ and $|\delta_l| > 1$. If the vertical component of the Hertz vector is known, the vertical component of the electric field may be calculated by

$$E_z(r, \varphi, z) = (k^2 + \frac{\partial^2}{\partial z^2})\Pi(r, \varphi, z)$$

[14] For determination of the values of the parameters of the inhomogeneous impedance model of the waveguide channel Earth–ionosphere, we attracted known from publications [*Orlov et al.*, 2000] vertical profiles of the concentration $N_e(z)$ and effective collision frequency $\nu_e(z)$ of electrons. For the given frequency and angle of incidence of the electromagnetic wave at an inhomogeneous layer Ψ, the equation for the impedance matrix

$$\hat{\delta}_i = \begin{pmatrix} \delta^{(e)} & \delta_{12} \\ \delta_{21} & \delta^{(m)} \end{pmatrix}$$

is integrated numerically from a height of ∼100 km downward to ∼40 km, covering with a guaranty the region important for formation of the reflected from the ionosphere VLF field [*Galiuk et al.*, 1989; *Kirillov,* 1979, 1981]. We take the determination of the impedance in the form $\mathbf{E}_{tg} = Z_0\hat{\delta}_i[\mathbf{H}_{tg} \times \mathbf{n}]$, where $Z_0 = \sqrt{\mu_0/\varepsilon_0}$, and $\mathbf{E}_{tg}$ and $\mathbf{H}_{tg}$ are the tangential to the considered surface components of the electric and magnetic fields, respectively. The values $\hat{\delta}_i = \hat{\delta}_d$ of the impedance matrix components obtained at the lower boundary of integration $z = z_d$ are recalculated to the height $z = h$ in the vacuum. The formulae for such recalculation we obtain using the following matrix of the reflection index of the plane wave

$$\hat{R} = \begin{pmatrix} R^{(e)} & R_{12} \\ R_{21} & R^{(m)} \end{pmatrix}$$

on the boundary of the plasma semispace in vacuum on the vertical coordinate

$$\hat{R}(z_d) = \hat{R}(h)\exp(2ik(h - z_d)\cos\Psi)$$

Substituting the relation of the reflection index and surface impedance matrix at the plasma semispace–vacuum boundary

$$R^{(e)}(z_d) = -\Big[\Big(\frac{\delta^{(e)}(z_d)}{\cos\Psi} - 1\Big)(\delta^{(m)}(z_d)\cos\Psi + 1) -$$

$$\delta_{12}(z_d)\delta_{21}(z_d)\Big]\xi_R$$

$$R_{12}(z_d) = -2\delta_{21}(z_d)\xi_R$$

$$R_{21}(z_d) = 2\delta_{12}(z_d)\xi_R$$

$$R^{(m)}(z_d) = \Big[\Big(\frac{\delta^{(e)}(z_d)}{\cos\Psi} + 1\Big)(\delta^{(m)}(z_d)\cos\Psi - 1) -$$

$$\delta_{12}(z_d)\delta_{21}(z_d)\Big]\xi_R$$

where

$$\xi_R =$$

$$\frac{\exp(2ikz_d\cos\Psi)}{\left(\frac{\delta^{(e)}(z_d)}{\cos\Psi} + 1\right)(\delta^{(m)}(z_d)\cos\Psi + 1) - \delta_{12}(z_d)\delta_{21}(z_d)}$$

into the expressions for the components of the impedance matrix, we obtain formulae for recalculation of the components of the impedance matrix to the height $z = h$ in vacuum

$$\delta^{(e)}(h) = \cos\Psi\times$$

$$\Big[(\exp(4ik\cos\Psi(h - z_d)) - 1)a_1^{(m)}(z_d)a_2^{(e)}(z_d) +$$

$$4\delta_{12}(z_d)\delta_{21}(z_d)\Big]\Big/\xi_\delta$$

$$\delta_{12}(h) = \frac{4\delta_{12}a_{12}\exp(2ik\cos\Psi(h - z_d))}{\xi_\delta}$$

$$\delta_{21}(h) = \frac{4\delta_{21}a_{12}\exp(2ik\cos\Psi(h - z_d))}{\xi_\delta}$$

$$\delta^{(m)}(h) = \frac{1}{\cos\Psi}\times$$

$$\Big[(\exp(4ik\cos\Psi(h - z_d)) - 1)a_2^{(m)}(z_d)a_1^{(e)}(z_d) +$$

$$4\delta_{12}(z_d)\delta_{21}(z_d)\Big]\Big/\xi_\delta$$

where

$$\xi_\delta = [\exp(2ik\cos\Psi(h - z_d)) - 1]^2 a_2^{(m)}(z_d)a_2^{(e)}(z_d) -$$

$$4\delta_{12}(z_d)\delta_{21}(z_d)$$

$$a_1^{(m)} = (\delta^{(m)}(z_d)\cos\Psi + 1)\times$$

$$\left[\frac{\delta^{(e)}(z_d)}{\cos\Psi} + i\tan(k\cos\Psi(h-z_d))\right] - \delta_{12}(z_d)\delta_{21}(z_d)$$

$$a_2^{(m)} = (\delta^{(m)}(z_d)\cos\Psi + 1)\times$$

$$\left[\frac{\delta^{(e)}(z_d)}{\cos\Psi} - i\cot(k\cos\Psi(h-z_d))\right] - \delta_{12}(z_d)\delta_{21}(z_d)$$

$$a_1^{(e)} = \left[\frac{\delta^{(m)}(z_d)}{\cos\Psi} + 1\right]\times$$

$$\left[\frac{\delta^{(e)}(z_d)}{\cos\Psi} + i\tan(k\cos\Psi(h-z_d))\right] - \delta_{12}(z_d)\delta_{21}(z_d)$$

$$a_2^{(e)} = \left[\frac{\delta^{(m)}(z_d)}{\cos\Psi} + 1\right]\times$$

$$\left[\frac{\delta^{(e)}(z_d)}{\cos\Psi} - i\cot(k\cos\Psi(h-z_d))\right] - \delta_{12}(z_d)\delta_{21}(z_d)$$

$$a_{12} = \left[\frac{\delta^{(e)}(z_d)}{\cos\Psi} + 1\right](\delta^{(m)}(z_d)\cos\Psi + 1) -$$

$$\delta_{12}(z_d)\delta_{21}(z_d)$$

[15] The height $z = h$ corresponds to the altitude where the combination of the impedance matrix $\delta = \delta^{(e)} - \delta_{12}\delta_{21}/\delta^{(m)}$ in a minimum way depends on the angle Ψ. For realization of such algorithm together with the equation for the matrix $\hat{\delta}_i$, the equation for its derivative $\partial\hat{\delta}_i/\partial\Psi$, is integrated. Also the formulae of recalculation of the derivative in vacuum were derived and used. The value of the Earth's surface impedance δ_g is determined by the given values of the relative dielectric permeability and conductivity for the two-layer model of the underlying surface.

[16] In this paper we are not interested in what degree the initial TM field at the scatter at the irregularity will be reexcited into the field of the TE polarization. We will assume this effect to be negligible. So the anisotropy related to the presence of the geomagnetic field will be approximately taken into account. It is known that in a general case the TM and TE components of the electric field are described by the electric $\Pi^{(e)}$ and magnetic $\Pi^{(m)}$ Hertz vectors and are related. For the field in the vacuum cavity this relation is expressed by the following boundary conditions at the ionospheric wall of the waveguide:

$$\frac{\partial}{\partial z}\begin{pmatrix} \Pi^{(e)} \\ Z_0\Pi^{(m)} \end{pmatrix} =$$

$$ik\begin{pmatrix} \delta^{(e)} - \dfrac{\delta_{12}\delta_{21}}{\delta^{(m)}} & \dfrac{-\delta_{12}}{\delta^{(m)}} \\ \dfrac{\delta_{21}}{\delta^{(m)}} & \dfrac{1}{\delta^{(m)}} \end{pmatrix} \times \begin{pmatrix} \Pi^{(e)} \\ Z_0\Pi^{(m)} \end{pmatrix}$$

So the impedance we use in the scalar problem is taken in the form

$$\delta_i = \delta = \delta^{(e)} - \frac{\delta_{12}\delta_{21}}{\delta^{(m)}}$$

3. Principal Equations

[17] Using the second Green formula one can obtain an expression for function $\Pi(r,\varphi,z)$ in any point of the D region via the integral over the irregularity surface $S_p \cup S_l$:

$$\Pi(\mathbf{R}) = \Pi_0(\mathbf{R}) + \frac{ik\varepsilon_0}{P_0}\int\limits_{S_p}\int \Pi(\mathbf{R}')\times$$

$$\left[\delta_p(r,\varphi)\Pi_0(\mathbf{R},\mathbf{R}') - \frac{\partial\Pi_0(\mathbf{R},\mathbf{R}')}{ik\partial z'}\right]dS' +$$

$$\frac{\varepsilon_0}{P_0}\int\limits_{S_l}\int \frac{\partial\Pi(\mathbf{R}')}{\partial n'}\left[\Pi_0(\mathbf{R},\mathbf{R}') - \frac{1}{ik\delta_l}\frac{\partial\Pi_0(\mathbf{R},\mathbf{R}')}{\partial n'}\right]dS_l' \quad (2)$$

where $\mathbf{R}(r,\varphi,z) \notin S_p, S_l$ denotes the observational point, $\mathbf{R}'(r',\varphi',z') \in S_p, S_l$ corresponds to the integration point, n' is the normal directed outside the wave volume, $\Pi_0(\mathbf{R})$ is the field of the initial source in a regular waveguide with a thickness of h and homogeneous walls with the impedances δ_g and δ_i, and $\Pi_0(\mathbf{R},\mathbf{R}')$ is the Green function. The expression for the latter may be obtained from the formula for $\Pi_0(\mathbf{R})$ substituting r by $r_1 = \sqrt{r^2 + r'^2 - 2rr'\cos(\varphi-\varphi')}$ and z_t by h (see Figure 1). In the limiting case $\mathbf{R} \to S_p, S_l$ in the right-hand side of equation (2), there appears an extra term of the form $\Pi(\mathbf{R})/2$, this fact being related to the jump in the normal derivative of the Green function $\partial\Pi_0(\mathbf{R}',\mathbf{R})/\partial n'$.

[18] This very choice of the Green function $\Pi_0(\mathbf{R},\mathbf{R}')$ in the form of a solution for the regular waveguide makes it possible to limit the region of integration in equation (2) down to the dimensions of the irregularity surfaces S_p and S_l. The method of construction of an approximate solution of equation (2) with the accuracy up to the terms of the order of $\mathbf{O}((kr)^{-1})$ was described in detail by *Soloviev* [1998]. The condition of its applicability is $kr \gg 1$ (that is, the observational point should be located in the wave zone from the source). There is no additional conditions, for example, on the dimensions of the irregularity. In this paper we describe only the main stages of the solution of equation (2).

[19] Two-dimensional equation (2) is solved by asymptotic transformation into an one-dimensional one. To do that we reveal the quickly oscillating multiplier and introduce the attenuation function

$$\Pi(\mathbf{R}) = \frac{P_0}{2\pi\varepsilon_0}\frac{\exp(ikr)}{r}V(\mathbf{R})$$

$$\Pi_0(\mathbf{R},\mathbf{R}') = \frac{P_0}{2\pi\varepsilon_0}\frac{\exp(ikr_1)}{r_1}V_0(\mathbf{R},\mathbf{R}')$$

If one introduces the ecliptic coordinates

$$r' = \frac{r}{2}(\cosh u + \cos\nu)$$

$$r_1 = \frac{r}{2}(\cosh u - \cos\nu)$$

$$dS' = r_1 r' du d\nu \qquad (-\infty < u < +\infty,\ 0 \le \nu \le \pi)$$

equation (2) for attenuation function would have the form

$$V(\mathbf{R}) = V_0(\mathbf{R}) + \frac{ikr}{2\pi} \times$$

$$\int\limits_{S_p} \int \left[\delta_p - \frac{1}{V_0(\mathbf{R},\mathbf{R}')} \frac{\partial V_0(\mathbf{R},\mathbf{R}')}{ik\partial z'} \right] \times$$

$$V(\mathbf{R}') V_0(\mathbf{R},\mathbf{R}') e^{ikr(\cosh u - 1)} du dv +$$

$$\frac{r\exp(-ikr)}{2\pi} \int\limits_{S_l} \int \frac{\partial W(\mathbf{R}')}{\partial n'} \times$$

$$\left[W_0(\mathbf{R},\mathbf{R}') - \frac{1}{\delta_l} \frac{\partial W_0(\mathbf{R},\mathbf{R}')}{ik\partial n'} \right] dS_l'$$

[20] When $kr \gg 1$, the exponential multiplier in the first integral becomes quickly changing in the direction transverse to the propagation circuit on the background of the multiplier left under the integral.

$$f(u,v) = V(\mathbf{R}') V_0(\mathbf{R}\mathbf{R}') \left[\delta_p - \frac{1}{V_0(\mathbf{R}\mathbf{R}')} \frac{\partial V_0(\mathbf{R},\mathbf{R}')}{ik\partial z'} \right]$$

[21] The latter makes it possible to perform the calculation of the integral in terms of dv over the cylinder base by the stationary phase method. As a result the integral in terms of variable v, which may be considered as a curvature integral along the irregularity boundary. The contour of integration is passed clockwise. Thus, with an accuracy up to the terms of the order of $\mathbf{O}((kr)^{-1})$, we obtain the expression for the attenuation function

$$V(\mathbf{R}) = V_0(\mathbf{R}) + \frac{r\exp(-ikr)}{2\pi} \int\limits_{S_l} \int \frac{\partial W(\mathbf{R}')}{\partial n'} \times$$

$$\left[W_0(\mathbf{R},\mathbf{R}') - \frac{1}{\delta_l} \frac{\partial W_0(\mathbf{R},\mathbf{R}')}{ik\partial n'} \right] dS_l' +$$

$$\frac{\sqrt{kr/2}}{2\pi} \oint\limits_{\gamma_p} \exp[ikr(\cosh(u) - 1]\, G[u(v), v] dv \qquad (3)$$

where

$$G[u(v), v] = \sqrt{\pi} e^{i3\pi/4} f(0, v) w(e^{i3\pi/4} p) +$$

$$\frac{1}{p} \left[f(0,v) - \frac{f(u(v),v)}{\cosh[u(v)/2]} \right]$$

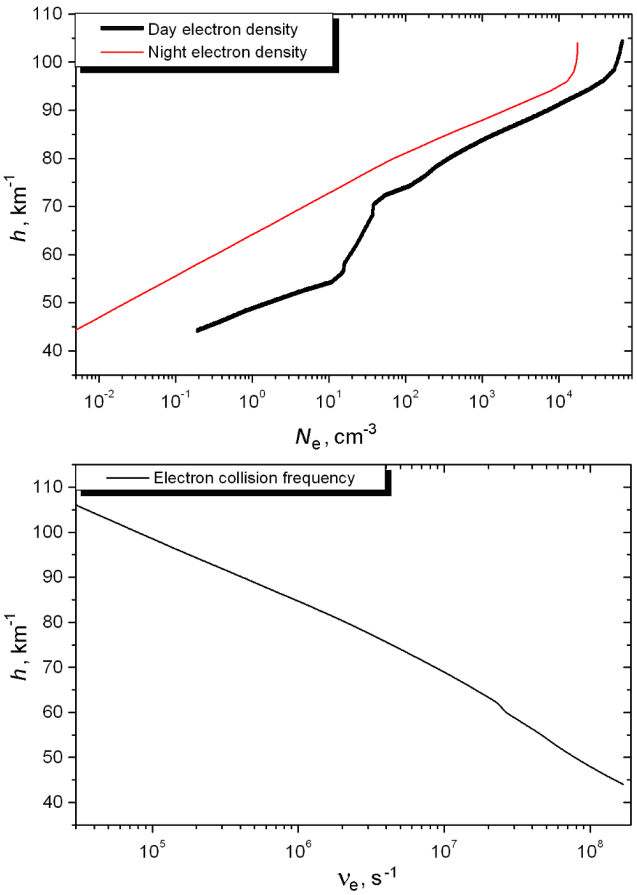

Figure 2. Vertical profiles of the concentration $N_e(z)$ and effective collision frequency $\nu_e(z)$ of electrons.

$$w(x) = e^{-x^2} \left(1 + \frac{2i}{\sqrt{\pi}} \int\limits_0^x \exp(t^2) dt \right)$$

$$p = \sqrt{2kr} \sinh[u(v)/2]$$

[22] To solve equation (3), we use the numerical-analytical method of semi-inversion [*Soloviev and Agapov*, 1997], which combines the direct inversion of the dominant part of the integral operator of the problem, that is a Volterra operator, with the iterative process by which the remaining part of the integral operator is inverted through successive approximations. The influence of the side surface of the cylindrical irregularity S_l is taken into account by convertional stepwise procedure. Below, all the results of numerical calculations are presented for the attenuation function $V(\mathbf{R})$. This function physically demonstrate the difference of the field in the waveguide with a three-dimensional irregularity from the dipole field over an ideally conducting surface.

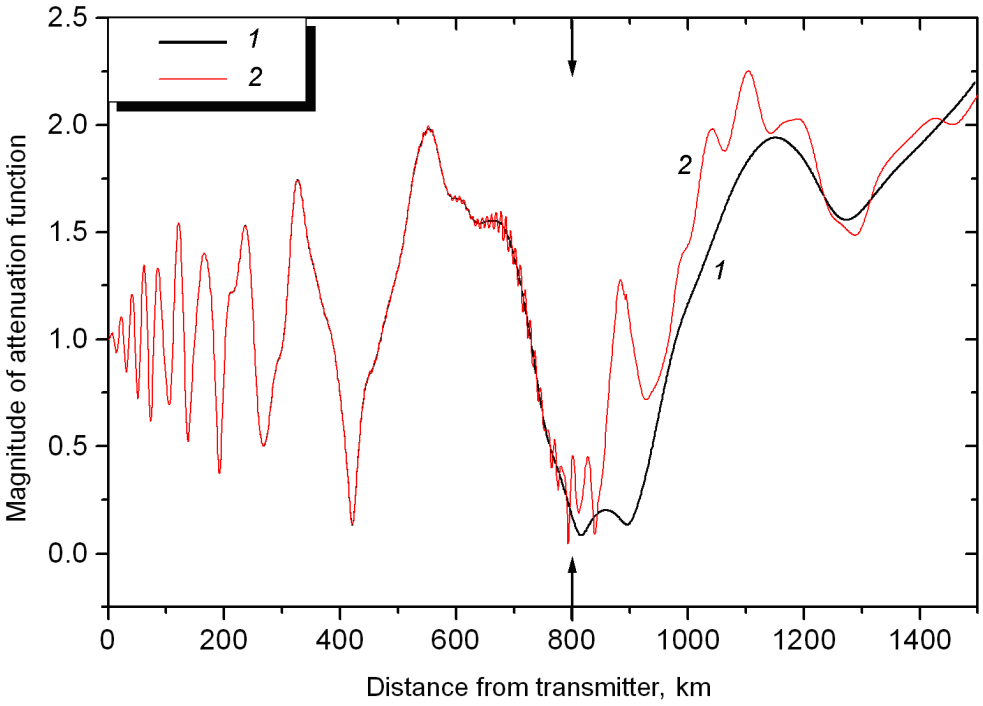

Figure 3. Amplitude of the attenuation function $V(x, y)$ for the nighttime period. Curves 1 and 2 correspond to a regular waveguide and a waveguide with local irregularity respectively.

4. Numerical Calculation Results

[23] As a result of the performed calculations, a series of regularities in the behavior of the amplitude and phase of the attenuation function $V(\mathbf{R})$ at the presence of a local irregularity at the upper wall of the Earth–ionosphere waveguide is found. It was assumed at calculations that the source and receiver are located on the Earth's surface: $z = z_t = 0$. The emitting frequency of the dipole was chosen to be $f = 20$ kHz. The height of the regular waveguide and its impedance were obtained using the vertical profiles of the concentration $N_e(z)$ and collision frequency $\nu_e(z)$ of electrons shown in Figure 2. The geomagnetic field was assumed to correspond to the mid-European conditions (in the vicinity of the point with coordinates 47°N and 18°E). The impedances of the base S_p and side surface S_l of the irregularity cylinder were chosen equal to $\delta_p = 0.5(1 + i)10^{-2}$ and $\delta_l = 0.5(1 - i)10^2$, respectively [*Soloviev and Hayakawa*, 2002]. The dimensions of the cross section of the cylinder (described by the formula $[(x - x_p)/a_p]^2 + [(y - y_p)/b_p]^2 = 1$, its height z_p, and location relative to the propagation path (shown in Figure 2 by arrows) determined by the coordinates of the ellipse center x_p and y_p were varied. Along the path $0 < x \leq 1500$ km the amplitude and phase of the attenuation function were calculated for the cases of various path orientation relative to the geomagnetic field vector, properties of the underlying surface, and location and geometric dimensions of the irregularity (a_p, b_p, and z_p).

[24] Figures 3 and 4 show the amplitudes and phases of the attenuation function for the nighttime period. The distance from the source to the receiver in kilometers is shown at the x axis. The underlying surface is wet soil with a relative dielectric permeability of $\varepsilon_m = 20$ and conductivity of $\sigma = 0.01$ S m^{-1}. The radio wave propagation direction is chosen along the south-north line (the azimuth is $A_z = 0$). The following parameters of the irregularity are chosen: $a_p = b_p = 20$ km and $z_p = 20$ km. In Figure 3 the irregularity is put directly over the signal propagation path ($y_p = 0$) in the region of the minimum of the attenuation function amplitude at the regular path ($x_p = 800$ km). At such choice of the coordinates, the effects related to the presence of the irregularity are best pronounced. It is demonstrated in Figure 4.

[25] No graphs of the amplitude and phase of the attenuation function for the daytime are presented in the paper. *Soloviev and Hayakawa* [2002] showed that such irregularities weakly distort the field in the daytime Earth–ionosphere waveguide. Moreover, the sprites modeled here are observed mainly at night.

[26] Below we consider the amplitude deviations: the difference in the attenuation function amplitude values in the undisturbed and disturbed by a three-dimensional irregularity cases. There exists an influence of the irregularity on the

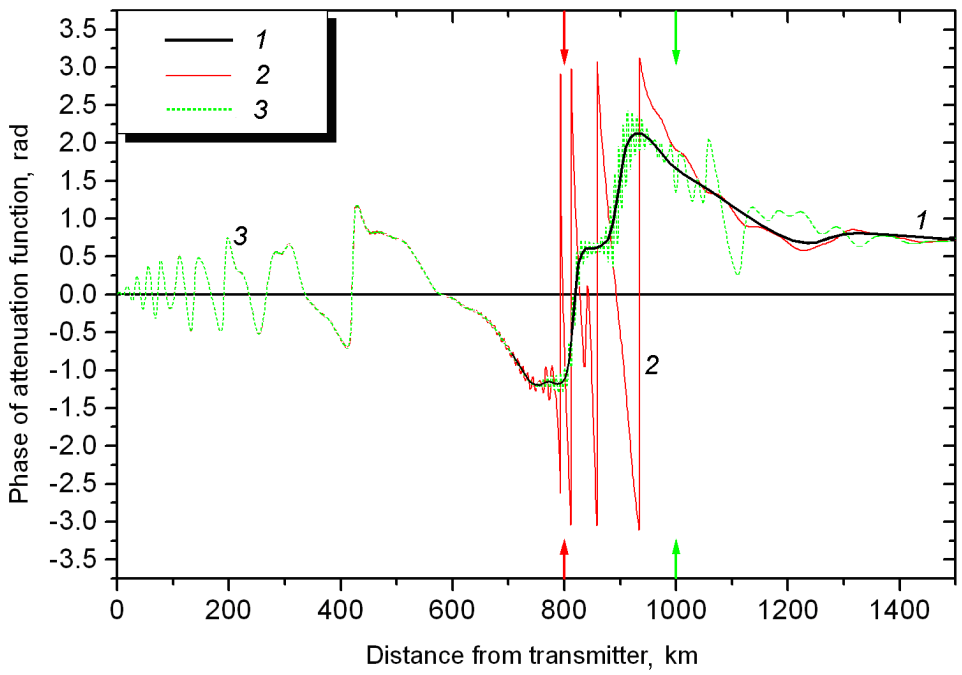

Figure 4. Phase of the attenuation function $V(x, y)$ for the nighttime period. Curve 1 corresponds to a regular waveguide, curves 2 and 3 correspond to a waveguide with local irregularity on the distance from receiver $x_p = 800$ and 1000 km, respectively.

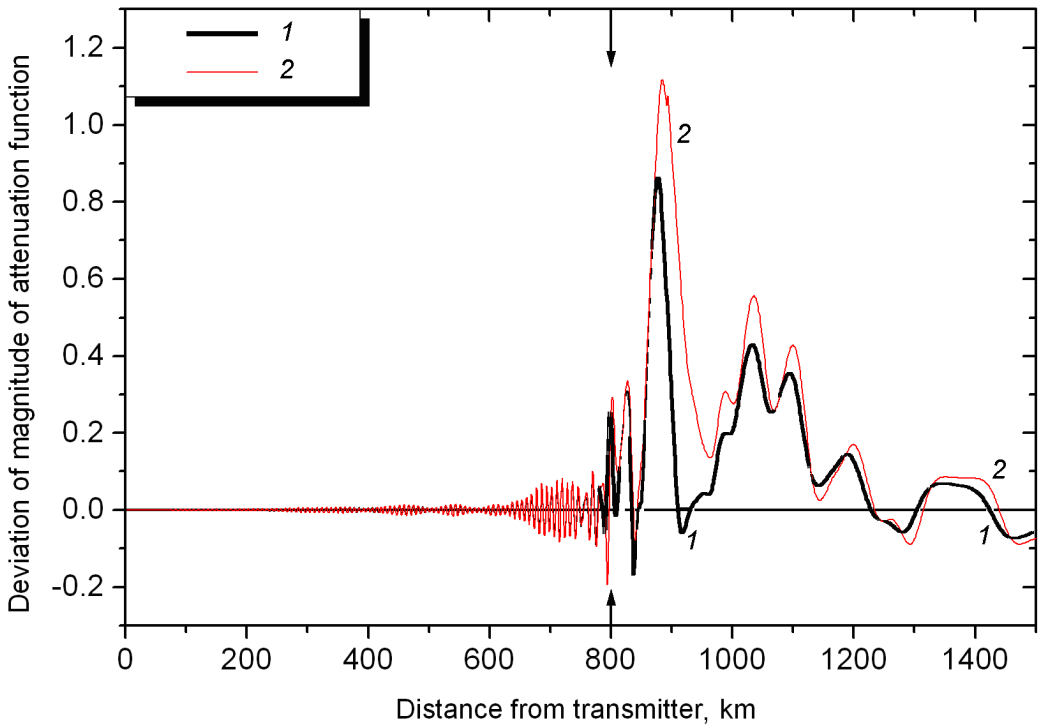

Figure 5. Perturbation of the amplitude of the attenuation function $V(x, y)$ caused by the presence of the irregularity. Curve 1 corresponds to the case when the geomagnetic field is not taken into account, and curve 2 corresponds to the magnetic azimuth of the propagation path $A_z = 0$. Parameters of the underlying surface are $\varepsilon_m = 20$ and $\sigma = 0.01$ S m^{-1}.

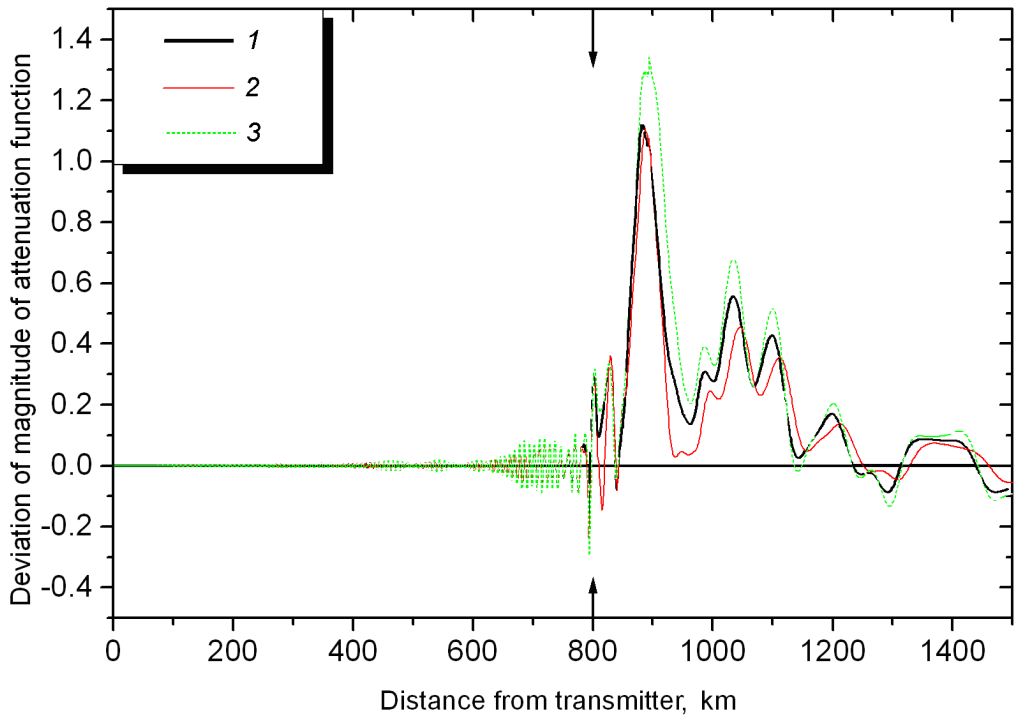

Figure 6. Perturbation of the amplitude of the attenuation function $V(x, y)$ in cases of various wave propagation path orientation relative to the geomagnetic field. Curves 1, 2, and 3 correspond to the path magnetic azimuths $A_z = 0$, $A_z = 90°$, and $A_z = -90°$, respectively.

behavior of the attenuation function phase, but it is less important than the influence on the amplitude behavior. Since the graphs showing the phase changes are not such visual as the graphs showing the amplitude changes, the former are not presented.

[27] Figure 5 shows the curves of amplitude disturbances corresponding to the cases when the geomagnetic field is and is not taken into account. The curves differ considerably from each other, so one may conclude that taking into account of the magnetic field is important. One can see in Figure 5 and the following figures the presence of not only forward scattering but backscattering as well.

[28] The perturbations in the attenuation function amplitude illustrating the influence of the irregularity on the field as a function of the propagation direction relative the magnetic azimuth of the path are shown in Figures 6 and 7. The strongest difference is seen between the field behavior at the paths with the azimuth $A_z = 90°$ and $A_z = -90°$, the former and the latter azimuths corresponding to the eastward and westward propagation, respectively. The change of the wave propagation direction to the opposite one ($A_z = 45°$ and $A_z = 225°$) is shown in Figure 7. It is worth noting that the presence of the irregularity influences these paths in a different way.

[29] Figures 8, 9, and 10 show the influence of the geometric dimensions of the irregularity on the attenuation function amplitude. Figure 8 shows curves corresponding to various values of the semiaxes of the cylinder base of the irregularity. The large and small semiaxes of ellipse are taken to be equal ($a_p = b_p$) and to have values of 10 km, 20 km, and 40 km. It is worth noting that a change of the radius of the cylinder base by a factor of 2 leads to a change in the maximum disturbance in the attenuation function amplitude approximately by the same factor.

[30] The influence of the cylinder height is shown in Figure 9. The values of the impedances of the base and sidewall of the cylinder stayed fixed. The comparison of the changes caused by the irregularity in the form of a cylinder with impedance of the base $\delta_p = 0.5(1 + i)10^{-2}$ and by the irregularity of a "spot" type with impedance $\delta_p = (2.38 - i \times 0.34)10^{-2}$ (obtained by recalculation to the waveguide height by the method described above) is shown in Figure 10. Comparing the curves one can conclude that taking into account of the possibility of a descent (assent) of the local region of the waveguide upper wall relative to the level of the regular ionosphere plays an important role in the study of the irregularity impact on radio wave propagation.

[31] Figure 11 illustrates the fact that the influence of the irregularity on the field in the waveguide depends also on the location of the irregularity relative to the radio wave prop-

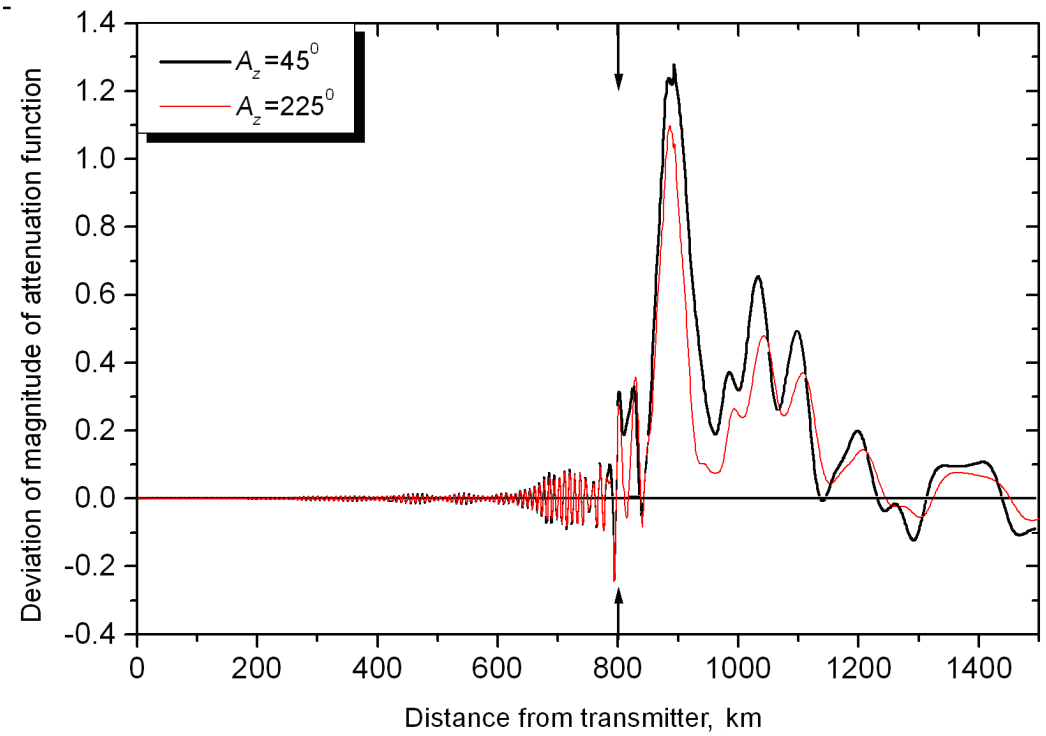

Figure 7. Perturbation of the amplitude of the attenuation function $V(x, y)$ at the reversal of the wave propagation direction ($A_z = 45^\circ$) to the opposite one ($A_z = 225^\circ$).

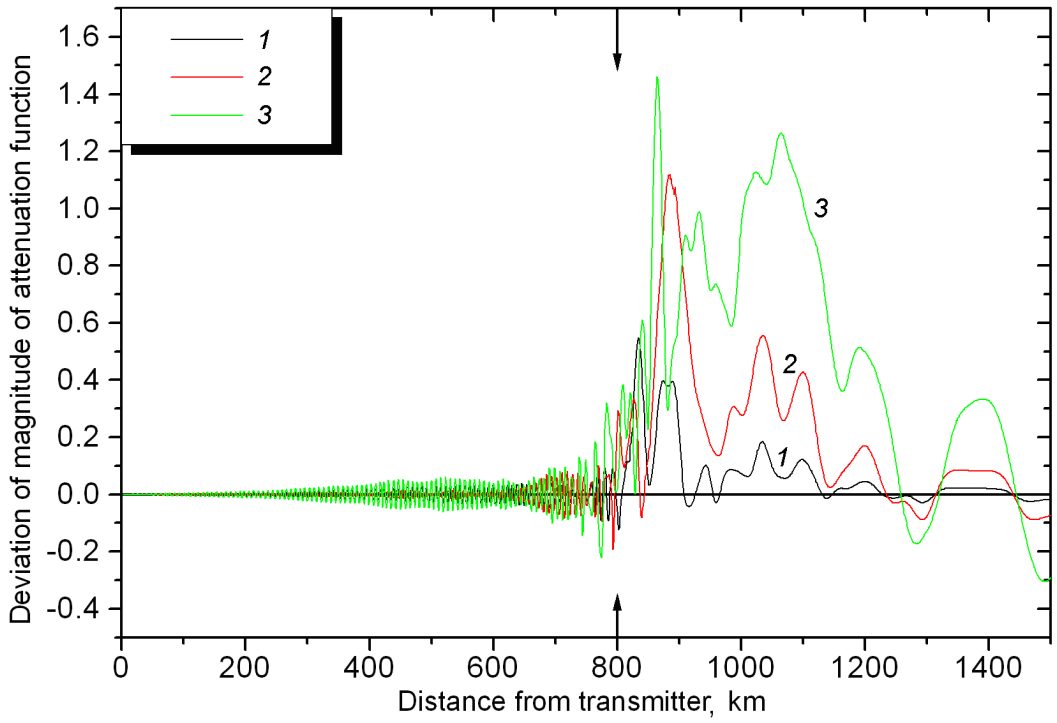

Figure 8. Perturbation of the amplitude of the attenuation function $V(x, y)$ at various dimensions of the cross section of the irregularity cylinder (a_p and b_p are the semiaxes of the base ellipse). Vertical dimension of the irregularity is $z_p = 20$ km.

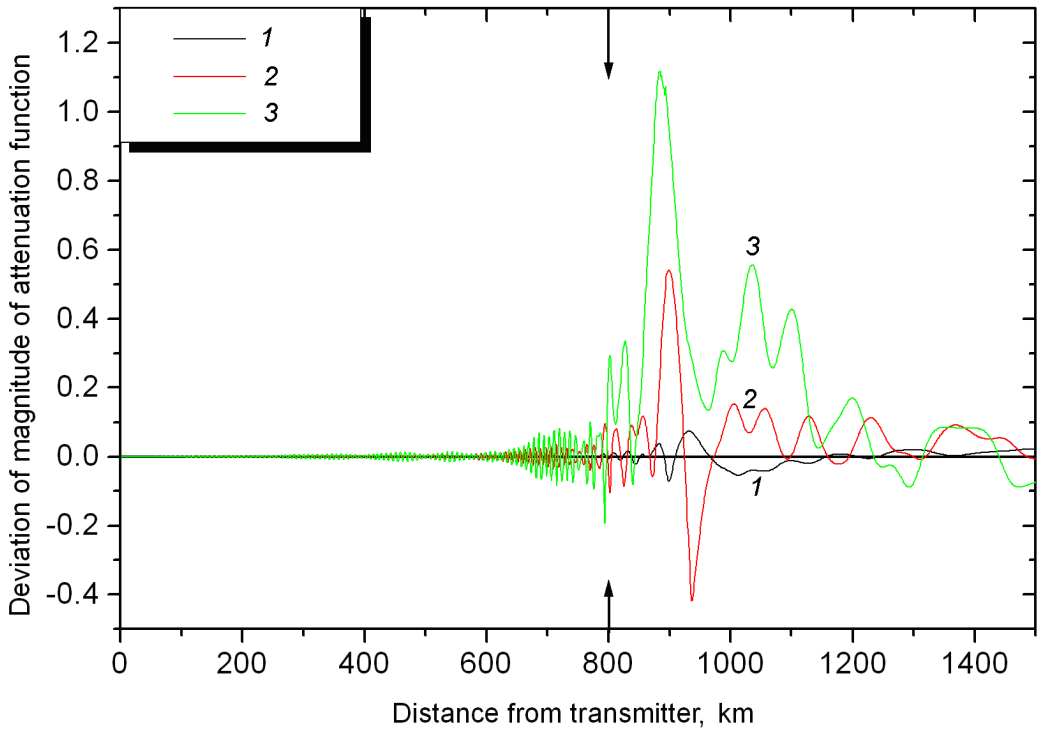

Figure 9. Influence of the cylinder height z_p on the amplitude perturbation. Curves 1, 2, and 3 correspond to $z_p = 0$ km, $z_p = 10$ km, and $z_p = 20$ km, respectively. The radius of the cylinder base is $a_p = b_p = 20$ km. The cylinder base impedance in all three cases is taken $\delta_p = 0.5(1 + i) \times 10^{-2}$.

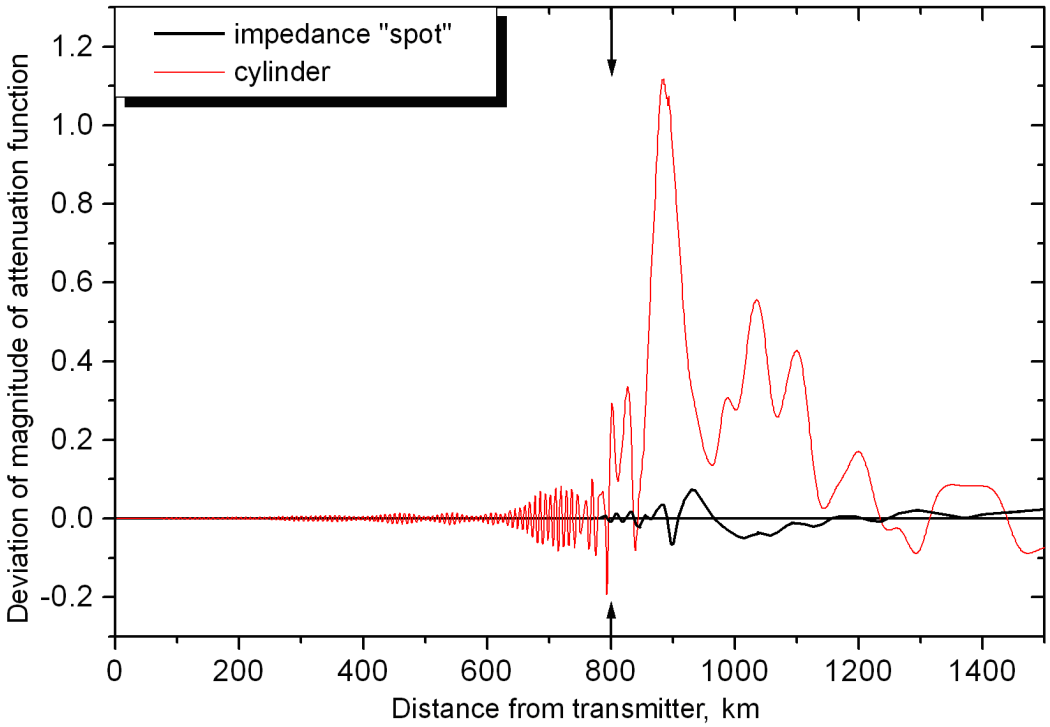

Figure 10. Perturbation of the amplitude of the attenuation function $V(x, y)$ in the cases "irregularity cylinder" ($\delta_p = 0.5(1 + i) \times 10^{-2}$, $z_p = 20$ km) and "irregularity spot" ($\delta_p = 2.38 - i0.34) \times 10^{-2}$, $z_p = 0$ km).

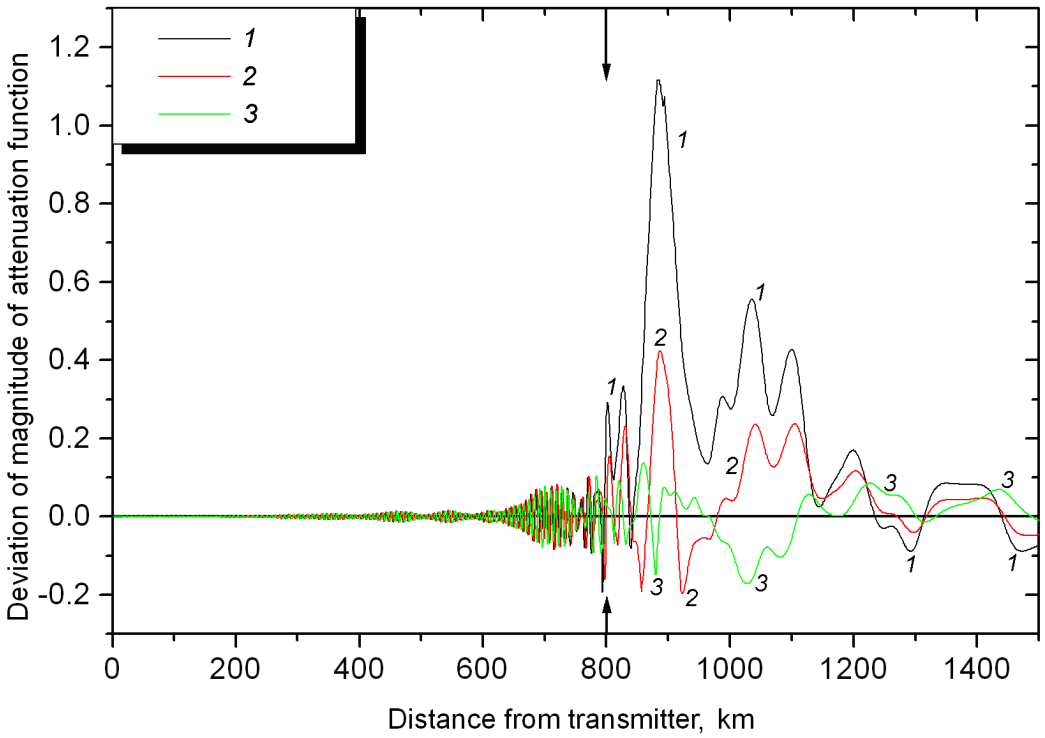

Figure 11. Perturbation of the amplitude of the attenuation function $V(x, y)$ at a shift of the irregularity location in the direction lateral to the propagation path by $y_p = 0$ km, $y_p = 20$ km, and $y_p = 50$ km (curves 1, 2, and 3 respectively). The coordinate along the path $x_p = 800$ km is the same for all three cases. Vertical dimension of the irregularity is $z_p = 20$ km.

agation path. Figure 11 shows the curves corresponding to the distance of the cylinder axis from the path line equal to $y_p = 0$, $y_p = 20$, and $y_p = 50$ km for $a_p = b_p = 20$ km and $x_p = 800$ km. At relatively short distances between the irregularity and path (∼50 km), a decrease of the maximum disturbance in the attenuation function amplitude by a factor of more than 10 is observed. It should be noted here that for the considered path, one can estimate the distance by the lateral dimension of the first Fresnel's zone, the small semiaxes of the latter being ∼53 km.

[32] The position of the observer influences considerably the estimate of the changes caused by the presence of the irregularity. A shift in the coordinates of the observational point actually corresponds to a shift in the irregularity location along and across the radio wave propagation path. The same shift in the direction lateral to the path would cause much stronger changes in the irregularity impact than a shift along the path. This dependence is shown in Figure 12.

[33] The influence of the underlying surface properties is shown in Figure 13. The curves are shown corresponding to the following underlying surfaces: wet soil ($\varepsilon_m = 20$, $\sigma = 0.01$ S m^{-1}) and seawater ($\varepsilon_m = 81$, $\sigma = 4$ S m^{-1}). Figure 13 shows the graph calculated at the value of the propagation path magnetic azimuth $A_z = 0$. It is worth noting that stronger influence of the irregularity is observed if a sea is the underlying surface than if waves propagate over a land. At other orientation of the wave propagation path, the character of the amplitude perturbations is the same.

5. Conclusions

[34] The performed studies make is possible to conclude on the degree of the influence of a local irregularity at the waveguide wall on radio wave propagation. The main goal of this paper is to give to an experimenter a possibility to estimate the scale of the expected changes in the amplitude and phase of the attenuation function. The analysis of the presented graphs shows at what parameters the obtained variations of the field are significant and can be detected experimentally. The study of the dependence of the irregularity on the propagation path orientation relative the geomagnetic field, properties of the underlying surface, location of the irregularity and its geometrical dimensions is performed. The analysis of the presented figures demonstrates the existence

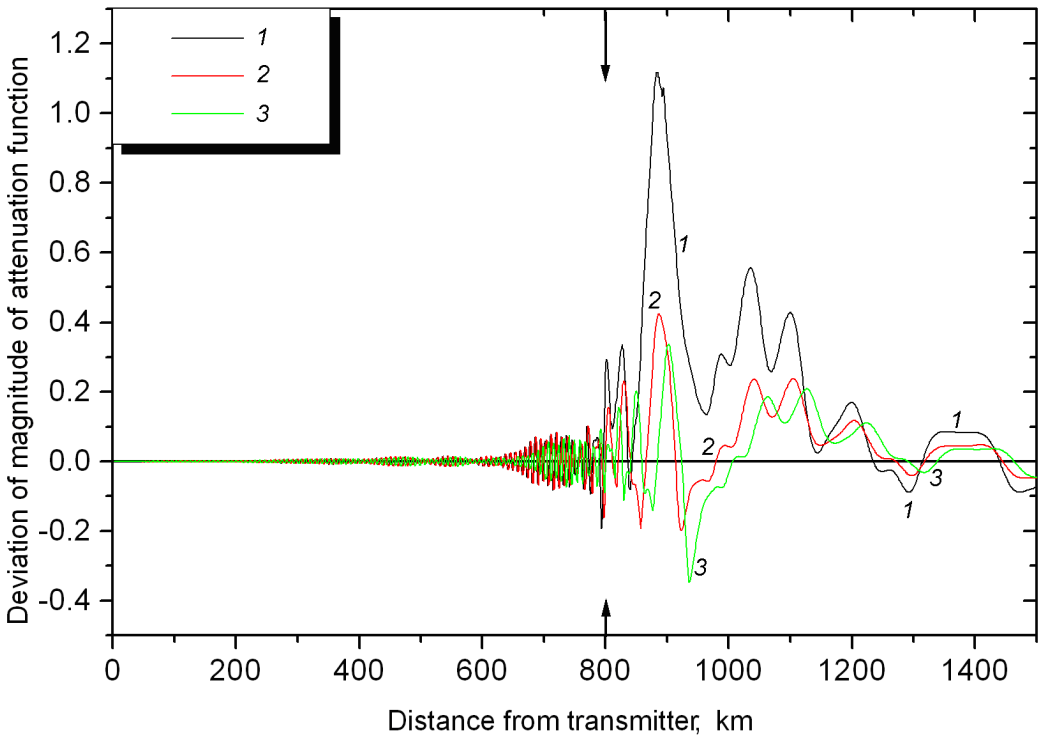

Figure 12. Perturbation of the amplitude of the attenuation function $V(x, y)$ at various location of the irregularity. Coordinates of the irregularity base center are $x_p = 800$ km, $y_p = 0$ km (curve 1); $x_p = 800$ km, $y_p = 20$ km (curve 2); and $x_p = 820$ km, $y_p = 20$ km (curve 3). The vertical dimension of the irregularity is $z_p = 20$ km.

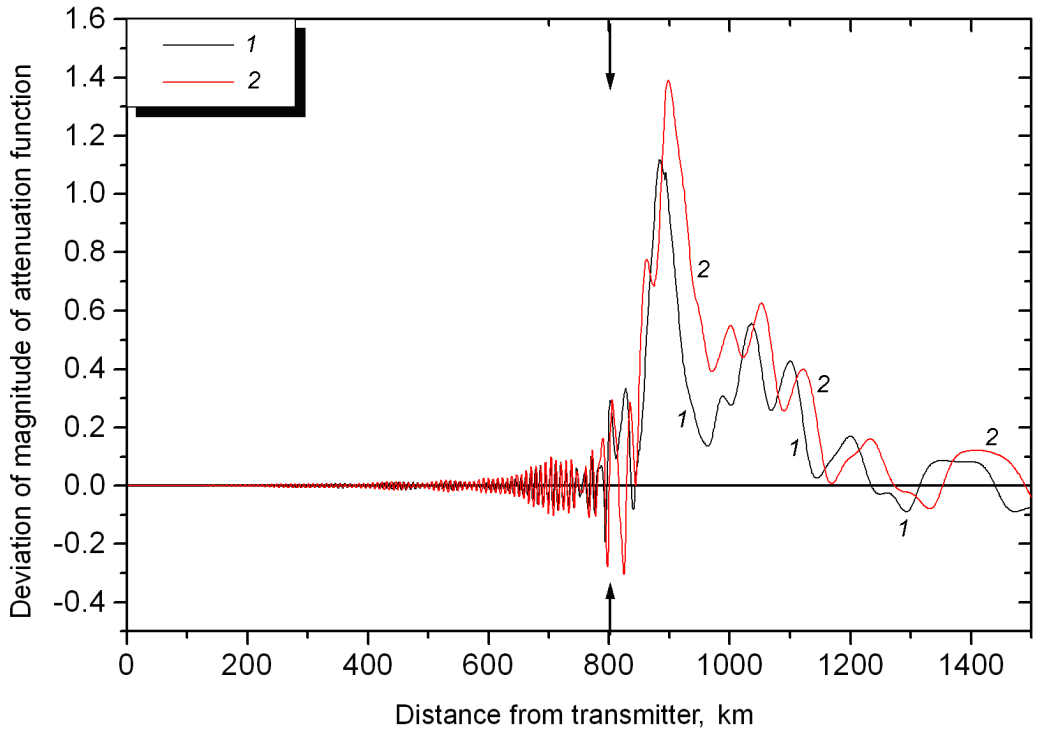

Figure 13. Influence of the underlying surface properties on perturbation of the amplitude of the attenuation function $V(x, y)$. The underlying surface is wet soil ($\varepsilon_m = 20$, $\sigma = 0.01$ S m^{-1}, curve 1) and seawater ($\varepsilon_m = 81$, $\sigma = 4$ S m^{-1}, curve 2). Magnetic azimuth of the propagation path is $A_z = 0$.

of the field scattered, not only forward, but the backscatter, as well, obtained on the basis of the theoretical calculations, allows us to expect its experimental registration.

[35] **Acknowledgments.** The authors thank V. I. Ivanov for his help in developing the program of impedance integration over the inhomogeneous ionosphere and V. V. Kirillov for useful advises and attention to this work.

References

Boccippio, D. J., E. R. Williams, S. J. Heckman, W. A. Lyons, I. T. Baker, and R. Boldi (1995), Sorites, ELF transients and positive ground strokes, *Science, 269,* 1088.

Boeck, W. L., O. H. Vaughan, Jr., R. Blakeslee, B. Vonnegut, M. Brook, and J. McKune (1995), Observations of lighting in the stratosphere, *J. Geophys. Res., 100*(D1), 1465, doi:10.1029/94JD02432.

Dowden, R. L., and C. J. Rodger (1997), Decay of vertical plasma column: A model to explain VLF sprites, *Geophys. Res. Lett., 24*(22), 2765, doi:10.1029/97GL02822.

Dowden, R. L., C. D. D. Adams, J. B. Brundell, and P. E. Dowden (1994), Rapid onset, rapid decay (RORD), phase and amplitude perturbation of VLF subionospheric transmission, *J. Atmos. Terr. Phys., 56*(11), 1513, doi:10.1016/0021-9169(94)90118-X.

Dowden, R. L., J. B. Brundell, and W. A. Lyons (1996), Are VLF rapid onset, rapid decay perturbations produced by scattering of sprite plasma?, *J. Geophys. Res., 101*(D14), 175, doi:10.1029/96JD01346.

Dowden, R. L., S. Hardman, J. Brundell, J. Bahr, Z. Kawasaki, and K. Nomura (1997), Red sprites observed in Australia, *IEEE Antennas Propagat. Mag., 39*(6), 106.

Franz, R. C., R. J. Nemzek, and J. R. Winckler (1990), Television image of a large upward electrical discharge above a thunderstorm system, *Science, 249,* 48.

Fukunishi, H., Y. Takahashi, M. Kubota, K. Sakanoi, U. S. Inan, and W. A. Lyons (1996a), Elves: Lighting-induced transient luminous events in the low ionosphere, paper presented at the 10th International Conference on Atmospheric Electricity, Int. Comm. on Atmos. Electr., Osaka, Japan.

Fukunishi, H., Y. Takahashi, M. Kubota, K. Sakanoi, U. S. Inan, and W. A. Lyons (1996b), Elves: Lighting-induced transient luminous events in the low ionosphere, *Geophys. Res. Lett., 23*(16), 2157, doi:10.1029/96GL01979.

Galiuk, Yu. P., A. B. George, and V. V. Kirillov (1989), Position of the effective ionospheric reflecting layer for electromagnetic ELF waves, *Problems Diffr. Propagat.* (in Russian), *22,* 85.

Helliwell, R. A., J. P. Katsufrakis, and M. L. Trimpi (1973), Whistler-induced amplitude perturbation in VLF propagation, *J. Geophys. Res., 78,* 4679.

Inan, U. S., D. C. Shafer, W. Y. Yip, and R. E. Orville (1988), Subionosphiric VLF signature of nigh-time D region perturbations in the vicinity of lighting discharges, *J. Geophys. Res., 93,* 455.

Inan, U. S., T. F. Bell, and J. V. Rodriguez (1991), Heating and ionization of the low ionosphere by lighting, *Geophys. Res. Lett., 18,* 705.

Inan, U. S., T. F. Bell, V. P. Pasko, D. D. Sentman, E. M. Wescott, and W. A. Lyons (1995), VLF signatures of ionospheric disturbances associated with sprites, *Geophys. Res. Lett., 22*(24), 3461, doi:10.1029/95GL03507.

Inan, U. S., W. A. Sampson, and Y. N. Tarasenko (1996), Space-time structure of optical flashes and ionization changes produced by lighting-EMP, *Geophys. Res. Lett., 23*(2), 133, doi:10.1029/95GL03816.

Kirillov, V. V. (1979), A method of calculation of VLF vertical electric dipole field in the Earth-ionosphere waveguide, *Problems Diffr. Propagat.* (in Russian), *17,* 57.

Kirillov, V. V. (1981), Electromagnetic waves in the thin spherical waveguide with anisotropic impedance walls, *Problems Diffr. Propagat.* (in Russian), *19,* 30.

Lyons, W. A. (1994), Characteristics of luminous structures in the stratosphere above thunderstorms as imaged by low-light video, *Geophys. Res. Lett., 21*(10), 875, doi:10.1029/94GL00560.

Lyons, W. A. (1996), Sprite observations above the U.S. high plains in relation to their parent thunderstorm system, *J. Geophys. Res., 101*(D23), 641, doi:10.1029/96JD01866.

Nunn, D. (1996), On the numerical modelling of the VLF Trimpi effect, *J. Atmos. Terr. Phys., 59,* 537.

Orlov, A. B., A. E. Pronin, and A. N. Uvarov (2000), The electron density of lower ionosphere profile modelling according to the VLF propagation data, *Problems Diffr. Propagat.* (in Russian), *28,* 83.

Pasko, V. P., U. S. Inan, T. F. Bell, and Y. N. Tarasenko (1997), Sprites produced by quasi-electrostatic heating and ionization in the low ionosphere, *J. Geophys. Res., 102*(A3), 4529, doi:10.1029/96JA03528.

Rairden, R. L., and S. B. Mende (1995), Time resolved sprite imagery, *Geophys. Res. Lett., 22*(24), 3465, doi:10.1029/95GL03332.

Rodger, C. J. (1999), Red sprites, upward lighting, and VLF perturbations, *Rev. Geophys., 37*(3), 317, doi:10.1029/1999RG900006.

Rodger, C. J. (2003), Subionospheric VLF perturbation associated with lighting discharges, *J. Atmos. Terr. Phys., 65*(5), 591, doi:10.1016/S1364-6826(02)00325-5.

Rowland, H. L., R. F. Fernsler, J. D. Huba, and P. A. Bernhardt (1995), Lighting driven EMP in the upper atmosphere, *Geophys. Res. Lett., 22*(4), 361, doi:10.1029/95GL00012.

Rycroft, M. J. (1973), Enhanced energetic electron intensities at 100 km altitude and a whistler propagating through the plasmasphere, *Planet. Space Sci., 21*(2), 239, doi:10.1016/0032-0633(73)90009-3.

Sentman, D. D., and E. M. Wescott (1995), Red sprites and blue jets: Thunderstorm-excited optical emission in the stratosphere, mesosphere, and ionosphere, *Phys. Plasmas, 2*(6), 2514, doi:10.1063/1.871213.

Soloviev, O. V. (1990), On the solution to the propagation problem for the locally irregular waveguide, *Radiophysics* (in Russian), *33*(9), 1078.

Soloviev, O. V. (1998), Low frequency radio wave propagation in the Earth-ionosphere waveguide perturbed by a large-scale three-dimensional irregularity, *Radiophysics, 41*(5), 588.

Soloviev, O. V., and V. V. Agapov (1997), An asymptotic three-dimensional technique to study radio wave propagation in the presence of a localized perturbation of environment, *Radio Sci., 32*(2), 515, doi:10.1029/96RS02919.

Soloviev, O. V., and M. Hayakawa (2002), Three-dimensional subionospheric VLF field diffraction by a truncated highly conducting cylinder and its application to Trimpi effect problem, *Radio Sci., 37*(5), 1079, doi:10.1029/2001RS002499.

Stenbaek-Nilsen, H. C., D. R. Moundry, E. M. Wescott, D. D. Sentman, and F. T. Sao (2000), Sprites and possible mesospheric effects, *Geophys. Res. Lett., 27*(23), 3829, doi:10.1029/2000GL003827.

Uman, M. A. (1987), *The Lighting Discharge, Int. Geophys. Ser., vol. 39,* Elsevier, New York.

Valdivia, J. A., G. M. Milikh, and K. Papadopoulos (1997), Red sprites: Lightings as a fractal antenna, *Geophys. Res. Lett., 24*(24), 3169, doi:10.1029/97GL03188.

Vaughan, O. H., Jr., R. Blakeslee, W. L. Boeck, B. Vonnegut, M. Brook, and J. McKune, Jr., (1992), A cloud-to-space lighting as recorded by the space shuttle payload-bay camera, *Mon. Weather Rev., 35*(7), 1459, doi:10.1175/1520-0493(1992)120¡1459:ACTSLA¿2.0.CO;2.

Wescott, E. M., D. D. Sentman, M. J. Heavner, D. L. Hampton, D. L. Osborne, and O. H. Vaughan, Jr., (1996), Blue

starters: Brief upward discharges from an intense Arkansas thunderstorm, *Geophys. Res. Lett., 23*(16), 2153, doi:10.1029/96GL01969.

Winckler, J. R. (1995), Further observations of cloud-ionosphere discharges above thunderstorms, *J. Geophys. Res., 100*(D7), 14,335, doi:10.1029/95JD00082.

Winckler, J. R., W. A. Lyons, T. E. Nelson, and R. J. Nemzek (1996), New high-resolution ground-based studies of sprites, *J. Geophys. Res., 101*(D3), 6997, doi:10.1029/95JD03443.

E. V. Moskaleva and O. V. Soloviev, Institute of Radio Physics, St. Petersburg State University, 1/1 Ul'yanovskaya Str., St. Petersburg, Petrodvoretz 198504, Russia. (moelvi@niirf.spbu.ru)